Combined Variable Speed Limit and Lane Change Control for Highway Traffic

Yihang Zhang and Petros A. Ioannou, *Fellow, IEEE*

***Abstract*— Variable speed limit (VSL) control of highway traffic is expected to improve traffic mobility, safety, and environment, especially during incidents. However, most existing VSL controllers show significant benefits in macroscopic analysis but little improvement in microscopic simulations in terms of traffic mobility. We demonstrate that the lack of improvement for travel time in many incident cases is due to lane changes that are taking place close to the bottleneck leading to severe capacity drop, which is not adequately captured by most macroscopic models. In this paper, we develop a combined lane change and VSL control scheme, which generates consistent improvements both with macroscopic and microscopic models. The lane change controller generates lane change recommendations upstream the incident or bottleneck in order to reduce the effect of the capacity drop. The VSL controller is developed using a feedback linearization approach based on the cell transmission macroscopic model and is shown analytically to guarantee exponential convergence to the optimum equilibrium point. Microscopic Monte Carlo simulations of traffic on the I-710 freeway were used to demonstrate that this combined control strategy is able to generate consistent improvements with respect to travel time, safety, and environmental impact under different traffic conditions and incident scenarios.**

***Index Terms*— VSL, lane change, feedback linearization.**

I. Introduction

HIGHWAY congestion is detrimental to traffic mobility, safety and the environment. Improving the efficiency of existing physical road infrastructure through the use of intelligent transportation technologies is an approach that continues to attract a lot of interest in research and industry. Variable Speed Limit (VSL) control is one of the widely studied highway traffic control technologies. Different VSL control methods have been designed and analyzed with the objective of improving traffic mobility, safety and impact on environment by adjusting speed limits upstream of incidents and bottlenecks [1]–[16].

Previous studies have shown improvements in traffic safety and the environment by using VSL [7], [11]–[14], [16]. However, inconsistent improvements have also been reported with respect to traffic mobility gains for different traffic scenarios and between theoretical macroscopic analysis and microscopic simulations or field tests [17]–[20]. Some references reported successful reductions in travel time by using different types of VSL controllers, which include model predictive control (MPC)-based VSL [2], [21], local feedback control-based [1], [4], [5], [8], [9], [22] and shockwave theory-based VSL [10]. In [23] the effect of VSL was studied using the fundamental diagram. The inability of VSL control techniques to consistently generate improvements with respect to travel time in microscopic simulations and field tests has been pointed out in [17]–[20].

Most researchers attribute the inconsistencies in travel time improvement to the highly disordered and stochastic traffic conditions at congested bottlenecks, which are difficult to predict with macroscopic models and regulate with VSL [17], [20], [24], [25].

One of the main factors of the disordered behavior at highway bottlenecks is the capacity drop phenomenon, where the maximum achievable traffic flow rate decreases when queues are formed [26], [27]. Under certain speed limit, when the density at the vicinity of the bottleneck increases to be higher than some critical value, a queue forms upstream of the bottleneck which decreases the capacity of the bottleneck. Capacity drop makes the dynamics of the traffic flow at bottleneck highly unstable, which is difficult for VSL control to maintain a high flow rate. Both MPC-based and local feedback-based VSL control methods have been proposed to maximize the flow rate at bottlenecks by considering the effects of capacity drop and some of the methods have shown significant improvement in mobility in both macroscopic and microscopic simulations, e.g., the Mainline Traffic Flow Control (MTFC) method [1] and the Link-Node Cell Transmission Model (LN-CTM) based MPC control [2]. The consistent results in [1] are achieved under the assumption that the capacity drop is introduced by ineffiecient acceleration of vehicles at the bottleneck, instead of the lane changes, which is not true in the case of incidents. The results in [2] are based on the assumption that once the VSL controller eliminates the capacity drop it does not occur again. While there is no reason to doubt the reported results, our studies and observations of traffic show clearly that forced lane changes in close proximity to the incident or bottleneck is the major cause of capacity drop and once it takes place VSL control will have limited or no effect in improving travel time. Most likely in the reported results which show significant benefits the scenarios did not involve significant forced lane changes or as in the case of [1] it was prevented by creating an

Manuscript received February 26, 2016; revised July 15, 2016; accepted October 2, 2016. This work was supported by the National Center for Sustainable Transportation, University of California at Davis, funded by the Department of Transportation. The Associate Editor for this paper was S. Sacone.

Y. Zhang is with the Department of Electrical Engineering, University of Southern California, Los Angeles, CA 90089 USA (e-mail: yihangzh@usc.edu).

P. A. Ioannou is with the Center for Advanced Transportation Technologies, University of Southern California, Los Angeles, CA 90089 USA (e-mail: ioannou@usc.edu).

Color versions of one or more of the figures in this paper are available online at http://ieeexplore.ieee.org.

Digital Object Identifier 10.1109/TITS.2016.2616493

acceleration area before the bottleneck. It should be intuitively clear that once the forced lane changes bring down the speed of vehicles in neighboring lanes there is no way for an VSL control technique to eliminate the capacity drop.

Some previous studies have confirmed the effect of lane changes in capacity drop or use lane management when designing the VSL controller [6], [7], [28], [29]. In [7], the authors of this paper used for the first time an adhoc combined variable speed limit and lane change (LC) control method to relieve congestion at highway bottlenecks. By providing appropriate lane change recommendations to upstream vehicles, most of the lane changes can be performed away from the incident hence capacity drop is dramatically reduced.

In this paper we use an analytical method to design a VSL controller based on a cell transmission macroscopic model with triangular fundamental diagram which together with a lane change controller guarantees stability of the traffic flow and convergence of traffic densities to that corresponds to optimum density and maximum flow with an exponential rate of convergence. In contrast to previous studies which relied on linearized models, our approach is based on feedback linearization and the results obtained are global. Therefore from the macroscopic point of view the proposed VSL and lane change control guarantees no capacity drop and maximum flow at the bottleneck. The lane change controller is based on a spatial model. In this case the control variable is the location of the lane change control commands. This location is found to depend on demand and number of lanes closed. The proposed combined lane change and VSL control design is evaluated using microscopic Monte Carlo simulations under different incident scenarios. The microscopic results generated are very consistent with the macroscopic ones and demonstrate consistent improvements in traffic mobility and impact on the environment for all the simulated scenarios.

The paper is organized as follows. Section II presents the model of the highway traffic system based on the cell transmission model. A feedback linearization VSL controller is proposed in Section III and shown to guarantee stability and exponential convergence to desired equilibrium point. In Section IV, we use both macroscopic and microscopic simulation results to examine consistency of results and evaluate benefits under different traffic flow scenarios and incidents using I-710 which involves passenger vehicles as well as trucks. Section V presents the conclusion.

II. System Modeling

A. Model of Highway Bottleneck

Consider a certain highway segment without on-ramps and off-ramps. A bottleneck is the point with lowest flow capacity. Due to the bottleneck a queue of vehicles forms as traffic demand increases. The flow rate of the bottleneck determines the throughput of the entire highway segment. Therefore, the modeling of the bottleneck traffic flow is crucial to the design of an efficient traffic control strategy. A bottleneck can be introduced by lane drop, incident lane blockage, merge point or other road conditions.

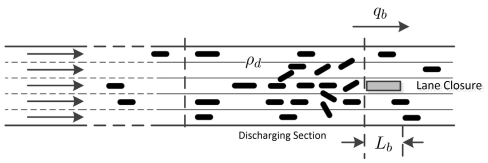

Fig. 1. Highway bottleneck.

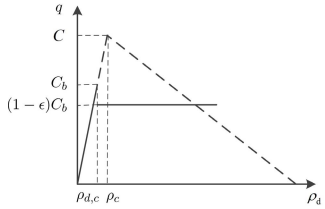

Fig. 2. Fundamental diagram.

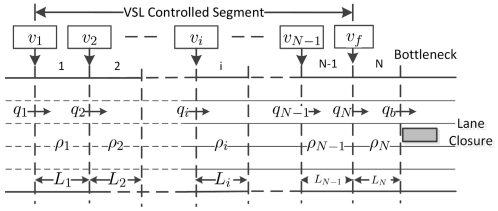

Fig. 3. Configuration of VSL control system.

Fig. 1 shows a highway segment with 5 lanes. A bottleneck is introduced by an incident which blocks one lane. The length of the bottleneck is denoted by L_b. We assume that the capacity of the highway segment before the incident is C. Then the ideal capacity of the bottleneck after the incident should be $C_\mathrm{b} = \frac{4}{5}C$. As we can see in Fig. 1, if L_b is small, the effect of the density within L_b is negligible and will not affect the bottleneck flow. The flow rate q_b at the bottleneck is determined by ρ_d, the vehicle density of the immediate upstream section of the bottleneck, which is referred to as the discharging section in Fig. 1. We adopt the assumption of triangular fundamental diagram, that is, when the value of ρ_d is low, $q_\mathrm{b} = v_\mathrm{f}\rho_\mathrm{d}$, where v_f is the free flow speed. However, when ρ_d is higher than some critical value $\rho_{\mathrm{d,c}}$, i.e. the demand of the bottleneck is higher than its capacity C_b, a queue forms at the discharging section which propagates upstream. Forced lane changes performed by the vehicles in the queue reduce the speed of flow in the open lanes. Therefore, the capacity would drop to $C'_\mathrm{b} = (1-\epsilon)C_\mathrm{b}$ once the queue forms [2], [3], [30]. The relationship between ρ_d and q_b is shown as solid line in Fig. 2 and is described by the equation

$$q_\mathrm{b} = \begin{cases} v_\mathrm{f}\rho_\mathrm{d}, & \rho_\mathrm{d} \le \rho_{\mathrm{d,c}} \\ (1-\epsilon)C_\mathrm{b}, & \rho_\mathrm{d} > \rho_{\mathrm{d,c}} \end{cases} \tag{1}$$

where $C_\mathrm{b} = v_\mathrm{f}\rho_{\mathrm{d,c}},\ \epsilon \in (0,1)$.

B. VSL Control Strategy and Cell Transmission Model

As shown in Fig. 3, the upstream highway segment of bottleneck is divided into N sections. The lengths of different

sections are expected to be similar but not necessarily identical. VSL signs are installed at the beginning of section 1 through section $N-1$. The speed limit in section N, which functions as the discharging section in Fig. 1, is constant and equals v_{f}, the maximum possible speed given by the fundamental diagram, which would let vehicles in open lanes get through the bottleneck as fast as possible, under the assumption of triangular fundamental diagram.

For $i = 1, 2, \ldots, N$, we denote the length, vehicle density and the inflow rate of section i with L_i, ρ_i and q_i respectively. For $i = 1, \ldots, N-1$, we denote the variable speed limit in section i with v_i. The variables ρ_i, q_i, v_i are all functions of time t. By conservation law, the dynamics of densities ρ_i are described by the differential equations

$$\begin{aligned} \dot{\rho}_i &= (q_i - q_{i+1})/L_i, \ i = 1, 2, \ldots, N-1 \\ \dot{\rho}_N &= (q_N - q_{\mathrm{b}})/L_N \end{aligned} \tag{2}$$

To obtain q_i, we use the cell transmission model proposed in [31]. Under the assumption of triangular fundamental diagram, we have:

$$\begin{aligned} q_1 &= \min\{d, C_1, w_1(\rho_{\mathrm{j},1} - \rho_1)\} \\ q_i &= \min\{v_{i-1}\rho_{i-1}, C_i, w_i(\rho_{\mathrm{j},i} - \rho_i)\}, \ i = 2, 3, \ldots, N \end{aligned} \tag{3}$$

where d is the demand flow of this highway segment assumed to be constant relative to the other variables. $\rho_{\mathrm{j},i}$ is the jam density of section i, at which q_i would be 0. w_i is the backward propagating wave speed in section i, C_i the capacity, i.e. the maximum possible flow rate in section i, given by $C_i = v_i w_i \rho_{\mathrm{j},i}/(v_i + w_i)$. We should note that for $i = N$, C_N and $\rho_{N,\mathrm{c}}$ are not the same as C_{b} and $\rho_{\mathrm{d,c}}$. When ρ_N reaches $\rho_{\mathrm{d,c}}$, q_{b} decreases but section N still has enough space for vehicles in section $N-1$ to flow in. Therefore, $\rho_{N,\mathrm{c}} > \rho_{\mathrm{d,c}}$, $C_N > C_{\mathrm{b}}$. The goal of the VSL controller is to stabilize the system described in (1) - (3) and maximize the flow rate q_{b}. According to (1), maximum q_{b} is obtained at $\rho_N = \rho_{\mathrm{b}}$, which is a discontinuity point of the fundamental diagram. From the macroscopic point of view, it is possible to find a VSL controller to maintain that $\rho_N = \rho_{\mathrm{d,c}}$ [3]. However, microscopic simulations in [7] demonstrate that when congestion occurs at the bottleneck, the queue accumulates so fast that VSL control can hardly reduce the density back to $\rho_{\mathrm{d,c}}$, therefore it fails to maintain maximum flow. The reason is explained in the following subsection.

C. Effects of Lane Change Control

In order to study the effect of lane change control, we build a hypothetical highway segment as shown in Fig. 1, which is straight, 8 km long and with 5 lanes, with the microscopic traffic flow simulated using the commercial software VISSIM [32]. The VISSIM model is calibrated with typical freeway road geometry and driving behavior. The bottleneck is formed by an incident which blocks the middle lane. We investigate the relationship between the flow of the bottleneck q_{b} and the density ρ_{d} in the 500 m long discharging section immediately upstream the bottleneck under different levels of traffic demand. Fig. 4 shows the relationship between

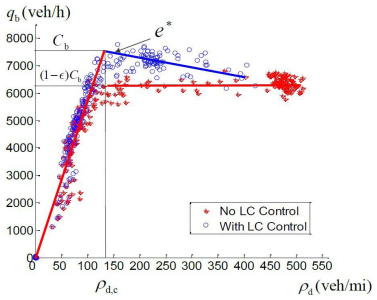

Fig. 4. Fundamental diagram with and without LC control.

q_{b} and ρ_{d} without any VSL control. The small blue circles describe the fundamental diagram in the case of lane change control. The red asterisks show the corresponding fundamental diagram in the absence of lane change control. The design procedure of LC controller is described in [7], and it is summarized in Section III-A for the sake of completeness.

Observing Fig. 4, we can see that when LC control is applied, the capacity of the bottleneck is around 7600 veh/h, which is achieved at $\rho_{\mathrm{d}} \approx 135$ veh/mi. However, when there is no LC control, q_{b} stops increasing even before ρ_{d} reaches 135 veh/mi (around ρ_{d} = 100 veh/mi). The highest flow rate is around 6300 veh/h. The reason why the flow rate in the no control case fails to reach higher level is demonstrated in Fig. 1. When vehicles approach the incident spot without being aware that their lane is blocked they are forced to slow down considerably and change lanes. These forced lane changes at low speed cause the traffic to slow down in the open lanes before and after the incident leading to lower volume, while the average density of the discharging section, ρ_{d}, is still low. Other parts of the fundamental diagram in the no control case fit equation (1) very well. Compared to the fundamental diagram with LC control, we can calibrate the parameters as, $\rho_{\mathrm{d,c}} = 135$ veh/mi, $C_{\mathrm{b}} = 7600$ veh/h and $\epsilon = 0.16$. The above stated behavior of the bottleneck makes it difficult for VSL control to increase q_{b} at the bottleneck, as VSL is only able to regulate the average density ρ_{d} in the discharging section, but cannot eliminate the forced lane changes at the vicinity of the bottleneck.

On the other hand, with the LC control, we can see that

1) no obvious capacity drop is observed at $\rho_{\mathrm{d}} = \rho_{\mathrm{d,c}}$;
2) q_{b} at $\rho_{\mathrm{d}} > \rho_{\mathrm{d,c}}$ is approximately linear with a negative slope w_{b}, which represents the wave propagation rate;
3) most data points scatter close to $\rho_{\mathrm{d}} = \rho_{\mathrm{d,c}}$. The points of high density are rare.

These observations show that the LC controller is able to reduce the number of vehicle stops in the queue at bottleneck and decrease the vehicle density, which makes the system continuous and easier for the VSL controller to stabilize. As a consequence of the LC control action, in the cell transmission model the relationship between ρ_N and q_{b} can be modeled as:

$$q_{\mathrm{b}} = \begin{cases} v_{\mathrm{f}}\rho_N, & \rho_N \le \rho_{\mathrm{d,c}} \\ w_{\mathrm{b}}(\rho_{\mathrm{j,d}} - \rho_N), & \rho_N > \rho_{\mathrm{d,c}} \end{cases} \tag{4}$$

where $\rho_{\mathrm{j,d}} = v_{\mathrm{f}}\rho_{\mathrm{d,c}}/w_{\mathrm{b}} + \rho_{\mathrm{d,c}}$.

Although the lane change control is able to recover the triangular shape of the fundamental diagram, when the demand is higher than the capacity C_b, a congestion will still occur at the bottleneck. Now the goal is to design a VSL controller to stabilize system (2) - (4) by homogenizing the densities in all sections and have them converge to an equilibrium which corresponds to the maximum possible flow as shown in the following section.

III. Design of the Combined VSL and LC Controller

A. Design of Lane Change Controller

The design of LC controller includes the pattern of the LC recommendation messages and the length of LC controlled segment. As we will explain below the control variable for LC control is the location of the LC recommendation which depends on a nonlinear spatial model that we developed.

1) Lane Change Recommendation Messages: Suppose a general highway segment has m lanes, with Lane 1 (Lane m) being the right (left) most lane in the direction of flow. We select the LC recommendation message R_i for lane $i, i = 1, 2, \ldots, m$ using the following rules:

1) For $1 \leq i \leq m$, if lane i is open, $R_i =$ "Straight Ahead";
2) For $i = 1 (i = m)$, if lane i is closed, $R_i =$ "Change to Left (Right)";
3) For $1 < i < m$, if lane i is closed, lane $i-1$ and lane $i+1$ are both open, $R_i =$ "Change to Either Side";
4) For $1 < i < m$, if lane i is closed, lane $i-1$ (lane $i+1$) is closed but lane $i+1$ (lane $i-1$) is open, $R_i =$ "Change to Left (Right)";
5) For $1 < i < m$, if lane i is closed, lane $i-1$ and lane $i+1$ are both closed, then we check R_{i-1} and R_{i+1}. If $R_{i-1} = R_{i+1}$, then $R_i = R_{i-1} = R_{i+1}$, else if $R_{i-1} \neq R_{i+1}$, $R_i =$ "Change to Either Side".

Rules (1)-(5) determine the LC recommendation messages depending on the incident location. The 5 rules covers all incident cases and are also mutually disjoint. Therefore they are well-defined and self-consistent.

2) Length of LC Control Segment: The control variables in the LC control case are the length of the LC control segment and the location of the LC recommendation. Within that segment, a LC recommendation is given at each section within the segment. The length of the LC controlled segment need to be long enough in order to provide adequate space and time for upstream vehicles to change lanes. Intuitively, if more lanes are closed at the bottleneck, a longer LC control distance is required. In addition, the capacity of the bottleneck and demand will also affect the LC control distance. On the other hand if the length of LC control segment is too long it may cause other problems as the blocked lane will appear empty to drivers inviting more lane changes in and out of the blocked lane which is going to deteriorate performance in terms of unnecessary maneuvers. We used extensive microscopic simulation studies to develop the following empirical model that allows us to generate the control variable d_{LC} which is the length of the LC controlled section given by the following equation:

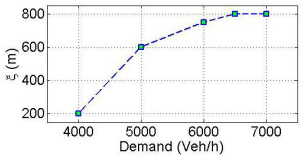

Fig. 5. ξ under different traffic demands.

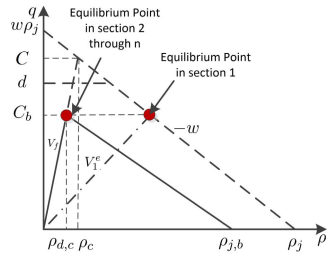

Fig. 6. Desired equilibrium point.

$$d_{LC} = \xi \cdot n, \tag{5}$$

where n is the number of lanes closed at the bottleneck, ξ a design parameter related to the capacity of bottleneck and the traffic demand which in our case is found to have the relationship shown in Figure 5. For a specific highway segment, the minimum value of ξ required under different traffic demands can be found by simulation. Since LC signs are only deployed at the beginning of sections, we choose the number of LC controlled sections M, as $M = \text{argmin} \left| \sum_{i=N-M+1}^{N} l_i - d_{LC} \right|$, where l_i represents the length of section i. More details can be found in [7]. Here we assume that the LC controlled segment has no on-ramp or off-ramps. The model (5) is empirical and more spacial than temporal despite the dependence of ξ on demand which may be time varying. The purpose of the LC control is to ask drivers to start changing lanes before the incident. It is an off and on controller i.e change lanes or not required to change lanes. It is different than the VSL controller which is purely dynamic.

B. Desired Equilibrium Point

The fundamental diagram under LC control is shown in Fig. 6. We consider the demand $d > C_b$, which may introduce congestion at the bottleneck. From the nonlinear system (2) - (4), we calculate the equilibrium point by setting the derivatives in (3)-(6) to be zero. Let $\rho^e = [\rho_1^e, \rho_2^e, \ldots, \rho_N^e]^T$ and $v^e = [v_1^e, v_2^e, \ldots, v_{N-1}^e]^T$ denote the vector of equilibrium density and the corresponding equilibrium speed limits in each section respectively. The desired equilibrium point should be the one at which maximum possible flow rate C_b is achieved and the upstream traffic flow is homogenized. According to the triangular fundamental diagram (4), since the speed limit is constant and equals v_f in section N, therefore the optimum equilibrium density for maximum flow is $\rho_N^e = C_b/v_f$. For section 2 through $N-1$, we set

$$\rho_2^e = \cdots = \rho_N^e = C_b/v_f, \;\; v_2^e = \cdots = v_{N-1}^e = v_f. \tag{6}$$

hence at the desired equilibrium point, the densities and speed limits in section 2 through N would be the same and the upstream traffic flow of the bottleneck is homogenized.

Since $d > C_{\mathrm{b}}$, we need to lower the speed limit in section 1 in order to suppress the traffic flow entering the controlled segment. According to (3), the equilibrium point satisfies:

$$v_1^{\mathrm{e}}\rho_1^{\mathrm{e}} = w_1(\rho_{\mathrm{j},1} - \rho_1^{\mathrm{e}}) = C_{\mathrm{b}}.$$

which gives

$$\rho_1^{\mathrm{e}} = \rho_{\mathrm{j},1} - C_{\mathrm{b}}/w_1,\ v_1^{\mathrm{e}} = C_{\mathrm{b}}w_1/(\rho_{\mathrm{j},1}w_1 - C_{\mathrm{b}}) \tag{7}$$

The equilibrium point described in (6) - (7) is the desired equilibrium point which maximizes the flow at the bottleneck and homogenizes the upstream traffic. In addition, it minimizes the average travel time according to the fundamental diagram. Without loss of generality, we assume the length of all sections are the same and equal to unit length. The system (2) - (4) can be expressed as follows:

$$\begin{aligned}
\dot\rho_1 &= w_1(\rho_{\mathrm{j},1} - \rho_1) - v_1\rho_1 \\
\dot\rho_i &= v_{i-1}\rho_{i-1} - v_i\rho_i,\ \text{for } i = 2,\dots,N-1 \\
\dot\rho_N &= \begin{cases} v_{N-1}\rho_{N-1} - v_{\mathrm{f}}\rho_N, & \rho_N \le \rho_{\mathrm{d,c}} \\ v_{N-1}\rho_{N-1} - w_{\mathrm{b}}(\rho_{\mathrm{j,b}} - \rho_N), & \rho_N > \rho_{\mathrm{d,c}} \end{cases}
\end{aligned} \tag{8}$$

In (8), the only switching point is $\rho_N = \rho_{\mathrm{d,c}}$. This is consistent with real-world, since the capacities of upstream sections are much larger than C_{b}. As long as system (8) converges to the desired equilibrium point, the steady-state bottleneck flow is maximized and upstream traffic is homogenized.

C. Feedback Linearization VSL Controller

For the design and analysis of the VSL controller we define the deviations of the state of (8) from the desired equilibrium (6) - (7) by defining the error system as: $e_i = \rho_i - \rho_i^{\mathrm{e}}$ for $i = 1, 2, , \dots, N$ and $u_i = v_i - v_i^{\mathrm{e}}$ for $i = 1, 2, \dots, N-1$. Substitute into (8), we have

$$\begin{aligned}
\dot e_1 &= -w_1 e_1 - v_1^{\mathrm{e}} e_1 - u_1\rho_1 \\
\dot e_i &= v_{i-1}^{\mathrm{e}} e_{i-1} + u_{i-1}\rho_{i-1} - v_i^{\mathrm{e}} e_i - u_i\rho_i \\
&\qquad\qquad \text{for } i = 2,\dots,N-1 \\
\dot e_N &= \begin{cases} v_{N-1}^{\mathrm{e}} e_{N-1} + u_{N-1}\rho_{N-1} - v_{\mathrm{f}} e_N, & e_N \le 0 \\ v_{N-1}^{\mathrm{e}} e_{N-1} + u_{N-1}\rho_{N-1} + w_{\mathrm{b}} e_N, & e_N > 0 \end{cases}
\end{aligned} \tag{9}$$

The transformation of (8) to (9) shifts the non zero equilibrium state of (8) to the zero equilibrium point of (9). The nonlinear terms in (9) are $u_i\rho_i$ for $i = 1, 2, ..., N-1$. Now the problem is to select u_1 through u_{N-1} in order to stabilize system (9) and force all the errors or deviations from the equilibrium state to converge to zero.

We introduce the following feedback controller which 'kills' all nonlinearities and forces the closed loop system to be linear, an approach known as feedback linearization [33]. We choose

$$\begin{aligned}
u_i &= (-v_i^{\mathrm{e}} e_i - \lambda_i e_{i+1})/\rho_i, \quad \text{for } i = 1,\dots,N-2 \\
u_{N-1} &= \begin{cases} \frac{-\lambda_{N-1}e_N - v_{N-1}^{\mathrm{e}} e_{N-1} + v_{\mathrm{f}} e_N}{\rho_{N-1}}, & e_N \le 0 \\ \frac{-\lambda_{N-1}e_N - v_{N-1}^{\mathrm{e}} e_{N-1} - w_{\mathrm{b}} e_N}{\rho_{N-1}}, & e_N > 0 \end{cases}
\end{aligned} \tag{10}$$

where $\lambda_i > 0$ for $i = 1, \dots, N-1$ are design parameters. This is a switching controller, whose switching logic is based on the value of e_N. Since we avoid the capacity drop by applying the LC control, the controller is continuous at the switching point. With the feedback linearization controller (10), the closed loop system becomes:

$$\begin{aligned}
\dot e_1 &= -w_1 e_1 + \lambda_1 e_2 \\
\dot e_i &= -\lambda_{i-1} e_i + \lambda_i e_{i+1}, \text{for } i = 2\dots, N-2 \\
\dot e_{N-1} &= \begin{cases} -\lambda_{N-2}e_{N-1} - \lambda_{N-1}e_N + v_{\mathrm{f}} e_N, & e_N \le 0 \\ -\lambda_{N-2}e_{N-1} - \lambda_{N-1}e_N - w_{\mathrm{b}} e_N, & e_N > 0 \end{cases} \\
\dot e_N &= -\lambda_{N-1} e_N
\end{aligned} \tag{11}$$

The stability properties of the closed loop system (11) are described by the following Theorem.

Theorem 1: The equilibrium point $e_i = 0$, $i = 1, 2, \dots, N$ of the system (11) is isolated and exponentially stable. The rate of exponential convergence depends on the control design parameters λ_i, $i = 1, 2, \dots, N-1$.

Proof: For $i = 1, 2, \dots, N$, setting $\dot e_i = 0$ in (11), the only equilibrium point is $e_i = 0$. From (11), we can see that the state e_N is decoupled from other states, i.e. $\dot e_N = -\lambda_{N-1}e_N$., whose solution is

$$e_N(t) = e_N(0)\exp(-\lambda_{N-1}t),\ \forall t > 0. \tag{12}$$

Since $\exp(-\lambda_{N-1}t) > 0$ for all t, $e_N(t)$ and $e_N(0)$ have the same sign for all $t > 0$, i.e. if $e_N(0) \le 0$, then $e_N(t) \le 0$, if $e_N(0) > 0$, then $e_N(t) > 0$ for all $t > 0$. In other words e_N is either non increasing or non decreasing which means that the state e_N will not switch between $e_N \le 0$ and $e_N > 0$. Therefore, the dynamics of state e_{N-1} can be written as

$$\dot e_{N-1} = \begin{cases} -\lambda_{N-2}e_{N-1} - \lambda_{N-1}e_N + v_{\mathrm{f}} e_N, & e_N(0) \le 0 \\ -\lambda_{N-2}e_{N-1} - \lambda_{N-1}e_N - w_{\mathrm{b}} e_N, & e_N(0) > 0 \end{cases}$$

Let us define $e = [e_1, e_2, \dots, e_N]^T$, then the system (11) can be written in the compact form

$$\dot e = \begin{cases} A_1 e, & e_N(0) \le 0 \\ A_2 e, & e_N(0) > 0 \end{cases} \tag{13}$$

where

$$A_i = \begin{bmatrix} -w_1 & \lambda_1 & & & & \\ & -\lambda_1 & \lambda_2 & & & \\ & & \ddots & \ddots & & \\ & & & -\lambda_{N-2} & -\lambda_{N-1} + \beta_i & \\ & & & & & -\lambda_{N-1} \end{bmatrix}, \quad i = 1, 2$$

and $\beta_1 = -w_{\mathrm{b}}$, $\beta_2 = v_{\mathrm{f}}$. A_1 and A_2 are both upper triangular matrices with all diagonal entries being negative real numbers, i.e. A_1, A_2 are both Hurwitz. Hence, system (13) is exponentially stable. Therefore (11) is also exponentially stable. In addition, for a given sign of $e_N(0)$ there is no switching taking place in (13).

The rate of convergence to the equilibrium depends on the design parameters $\lambda_i, i = 1, 2, ...N-1$ which can be tuned to achieve a desirable convergence rate. It would also depend on the sign of the initial condition $e_N(0)$ as the dynamics that drive the error system depend on whether the initial condition $e_N(0)$ is negative or positive. □

D. Constraints on VSL Commands

In Section III-C, we showed that the feedback linearization controller (10) forces the closed loop system (11) to be exponentially stable. This is under the assumption that the variable speed limit commands vary continuously. Since it is not possible for vehicle drivers to follow speed limits which vary continuously or too fast and since speed limits cannot be too high or too low for safety and implementation issues we apply the following constraints:

1) *Discretization in time.* We discretized the continuous time VSL control commands using the sampling period T_c so that the VSL command is kept constant to its value at $t = kT_c$ till $t = (k+1)T_c$ where $k = 0, 1, 2, \ldots$.
2) *Finite command space.* We use a quantization of 5 mi/h to truncate the generated VLS commands which is easy to follow.
3) *Saturation of Speed Limit Variations.* It is dangerous to decrease the speed limit too fast in both time and space. The decrease should be within some threshold $C_v > 0$ between successive control periods and highway sections. We don't bound the speed limit variation if the speed limit increases. In addition the VSL commands never exceed the legal speed limit.

Using the above constraints we modify the VSL control commands as follows:

Let $u_i(k)$ denotes u_i computed by equation (10) at $t = kT_c$. We have,

$$\bar{v}_i(k) = \left[v_i^e + u_i(k)\right]_5 \tag{14}$$

$$\tilde{v}_i(k) = \max\{\bar{v}_i(k), v_i(k-1) - C_v, v_{i-1}(k) - C_v\} \tag{15}$$

$$v_i(k) = \begin{cases} v_{\max}, & \text{if } \tilde{v}_i(k) > v_{\max} \\ v_{\min}, & \text{if } \tilde{v}_i(k) < v_{\min} \\ \tilde{v}_i(k), & \text{otherwise} \end{cases} \tag{16}$$

for $i = 1, 2, \ldots, N-1, k = 0, 1, 2, \ldots$.

In (14), $[\cdot]_5$ is the operator which rounds a real number to its closest whole 5 number. Equation (15) describes the saturation limits on the amount of decrease of VSL commands between successive control steps and highway sections. In (16), $v_{\max}$ and $v_{\min}$ are the upper and lower bounds of VSL commands respectively. The above modifications will influence the ideal performance of the VSL controller described by Theorem 1. Such modifications are necessary in every control application [1], [24], [34] and the way to deal with possible deterioration from the ideal performance is to use the design parameters $\lambda_1, \lambda_2, \ldots, \lambda_{N-1}$ to tune the system using intuition and practical considerations. The selection of the feedback gains $\lambda_1, \lambda_2, \ldots, \lambda_{N-1}$ has to consider the trade off between stability and robustness with respect to modeling errors.

E. Robustness With Respect to Varying Demands

In the analysis above, we assume that the demand d is a constant and $d > C_b$. As explained below, the proposed VSL controller is robust with respect to different demands.

If $d < C_b$, vehicles in the controlled segment would discharge and the densities in each section would be lower than the desired density. The VSLs in each section would increase, but saturated at v_f. This situation is easy as due to the low demand congestion can be avoided or managed very well.

When $d > C_b$ and keeps increasing, according to Theorem 1, the controller lowers the speed limit in section 1 and limits the number of vehicles that enter the downstream network. Therefore, a queue would be created whose size will be increasing upstream the flow. It appears, at first glance, as if we are moving congestion from the sections under VSL and LC control to upstream sections. The important question we need to answer is how many vehicles there are in this queue and how fast it grows with and without VSL and LC control in the sections under consideration.

In order to analyze the queue size upstream of section 1, we modify the system (2) - (4) by introducing a new state Q, which represents the number of vehicles in the queue upstream section 1. We assume that $Q = 0$ at steady state flow before the incident. Using the flow conservation equation, we have

$$\dot{Q} = d - q_1 \tag{17}$$

where d is the traffic demand. The inflow rate of section 1, q_1 then becomes

$$q_1 = \begin{cases} \min\{d, C_1, w_1(\rho_{j,1} - \rho_1)\}, & Q \le 0 \\ \min\{C_1, w_1(\rho_{j,1} - \rho_1)\}, & Q > 0 \end{cases} \tag{18}$$

Equation (18) assumes that as long as the queue upstream section 1 is not fully discharged, the inflow rate of section 1 will be as high as the maximum flow rate that section 1 can receive under current ρ_1. Note that the introduction of Q does not make any difference to system (2) - (4) before and during the incident. It only tracks the growth and discharge of the queue upstream section 1. Therefore the stability of the closed-loop system (11) is not affected.

Hence, with the combined VSL and LC controller, the queue size is measured with Q. In the no control case, a queue forms at section N, whose size is denoted by $\hat{Q}$. The following Lemma holds.

Lemma 1: If the demand $d > C_b$, $\hat{Q}$ grows faster than Q at steady state. In particular,

$$\dot{Q} - \dot{\hat{Q}} = -\epsilon C_b < 0 \tag{19}$$

Proof: Similar to Equation (17), we can estimate $\hat{Q}$ with the following equation $\dot{\hat{Q}} = d - \hat{q}_b$, where $\dot{\hat{Q}}$ is the growth rate of $\hat{Q}$, $\hat{q}_b$ is the outflow rate of section N without control. Since $d > C_b$, q_1 converges according to Theorem 1 to the desired flow rate C_b exponentially with the combined VSL and LC controller. $\hat{q}_b$ would decrease to $\hat{q}_b = (1-\epsilon)C_b$ due to capacity drop. Substituting the steady state values of q_1 and $\hat{q}_b$ in the above equations we obtain (19). i.e. at steady state, the growth rate of Q is less than that of $\hat{Q}$. □

From the analysis above, it is clear that if the demand d increases from below the bottleneck capacity C_b to greater than C_b and keeps increasing, the combined VSL and LC controller is able to protect the bottleneck from getting congested by suppressing the speed limit in section 1 therefore ρ_N can be stabilized at the desired value. On the other hand, in the no control case, the bottleneck is directly exposed to the excessive demand, therefore ρ_N increases and leads to

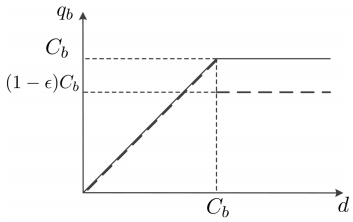

Fig. 7. Steady state q_b under different demands — with control, - - - without control.

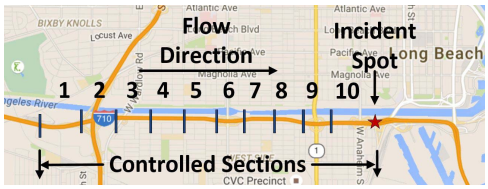

Fig. 8. Simulation network.

capacity drop. Fig. 7 plots the steady state bottleneck flow q_b with respect to demand d. When $d < C_b$, the bottleneck would not be congested. When $d > C_b$, the bottleneck flow would be stabilized at the maximum value C_b by the combined controller in the controlled case. In the no control case, the flow rate would decrease to $(1-\epsilon)C_b$ due to capacity drop.

Therefore, the combined VSL and LC controller is robust with respect to different levels of traffic demand. The queue of vehicles grows slower in the controlled case than in the case with no control.

IV. Numerical Simulations

In this section, we design and evaluate a combined VSL and LC controller for the simulation of a real world highway segment. We use both macroscopic and microscopic traffic flow models and carry out Monte Carlo simulations for different incident scenarios in order to evaluate consistency with respect to performance improvements.

A. Simulation Network and Scenarios

We evaluate the combined VSL & LC control method using a microscopic and macroscopic model of the traffic flow on a 10 mile (16 km)-long southbound segment of I-710 freeway in California, United States (between I-105 junction and Long Beach Port), which has a static speed limit of 65 mi/h (105 km/h). We build this freeway network in VISSIM and calibrate the microscopic model using historical data provided by [35]. The car following and lane change behavior of the VISSIM model is calibrated and validated using real measurements under static speed limit of 65 mi/h.

The highway segment under consideration has 3-5 lanes at different locations. Its normal capacity without an incident is about 6800 veh/h [35]. As shown in Fig. 8, we assume the bottleneck is introduced by an incident which blocks the middle lane in a 3-lane section, thus the ideal capacity of the bottleneck during incident is about 4500 veh/h. The upstream segment of the bottleneck is divided into ten 500 m-600 m sections. The bars across the highway in Fig. 8 indicate the locations where the VSL and LC signs are deployed.

To demonstrate the performance, robustness and consistency of the proposed controller under different incident conditions, we consider 3 different scenarios with different incident durations. We simulate each scenario under different demand flows. In each scenario, the incident occurs 5 minutes after simulation begins and lasts for **30 min** in scenario 1, which simulates the case of an incident of moderate duration which may be due to an accident; for **10 min** in scenario 2 which simulates the case of a short incident due to a vehicle breakdown or minor accident. The incident is **not removed** after occurrence in scenario 3, which simulates a long time lane closure or a construction site or a physical bottleneck. We evaluate the combined VSL and LC control performance for each scenario with constant demand flows of 6000 veh/h and 6500 veh/h which is higher than the capacity of the bottleneck.

B. Macroscopic Simulation

In this section, we use a macroscopic model to evaluate the performance of the proposed VSL controller. Since the macroscopic model used does not take into account lane changes and their effect close to the incident, we apply the LC controller to the corresponding microscopic model and use the microscopic model data to validate the macroscopic cell transmission model. The desired equilibrium point of the I-710 highway segment is calculated to be

$$\rho_1^{\mathrm{e}} = 174.6 \text{ veh/mi}, \ \rho_2^{\mathrm{e}} = \rho_3^{\mathrm{e}} = \cdots = \rho_{10}^{\mathrm{e}} = 90 \text{ veh/mi}$$
$$v_1^{\mathrm{e}} = 33.5 \text{ mi/h}, \ v_2^{\mathrm{e}} = v_3^{\mathrm{e}} = \cdots = v_9^{\mathrm{e}} = 65 \text{ mi/h}$$

The LC recommendation sign is deployed at the beginning of section 9 and section 10 in Fig. 8, and recommends vehicles to change lanes by moving to the open lanes on either side. For the VSL controller, the following parameters are used: $C_v = 10$ mi/h, $v_{\max} = 65$ mi/h, $v_{\min} = 10$ mi/h, $T_c = 30$ s. We choose $\lambda_1 = \lambda_2 = \cdots = \lambda_9 = 20$. We should note that as mentioned in Section IV-A, the capacity of the bottleneck with incident is 4500 veh/h. However, in the macroscopic model, we are assuming a strict triangular fundamental diagram and the capacity C_b is calibrated to be $v_f \times \rho_{10}^{\mathrm{e}} = 5850$ veh/h. The reasons for this difference are explained in the following section. Since the logic of our VSL controller is to stabilize the density at the critical value, the accurate value of equilibrium density is more important than the value of flow rate. The densities and variable speed limits for the case of scenario 1 with demand $d = 6500$ veh/h are plotted in Fig. 9. For clarity of presentation, we only plot the densities in section 1, 9 and 10 and VSL commands in section 1 and 9.

Fig. 9 demonstrates what is predicted by theory. That is the density in section 1 converges to the desired density of 174.6 veh/mi and the densities in sections 9, 10 to the desired density of 90 veh/mi till the incident is removed at $t = 35$ min, in which case the densities converge to 105 veh/h, which is higher than the pre-incident value. This is because the queue formed at section 1 during the incident needs to discharge,

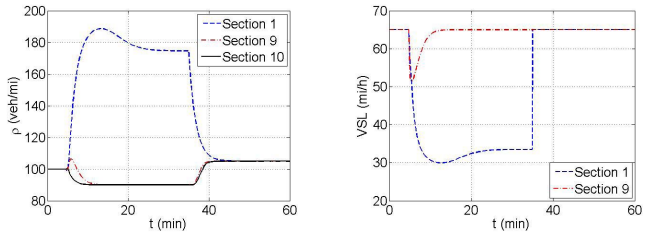

Fig. 9. Controller performance without constraints. (a) Vehicle Density. (b) VSL Command.

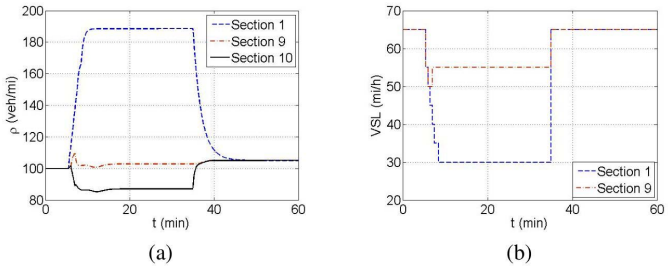

Fig. 10. Controller Performance with Constraints. (a) Vehicle Density. (b) VSL Command.

therefore the temporary demand of the bottleneck after the incident is higher than the demand of the overall network.

We then apply the constraints (14) - (16) to the VSL controller. The densities and VSL commands with constraints are shown in Fig. 10. Fig. 10a demonstrates that the density in the discharging section converges to $\rho_{10} = 85$ veh/mi, which is lower than $\rho_{10}^{e} = 90$ veh/mi. According to the fundamental diagram in Fig. 6, the steady state flow would be a bit lower than the desired flow rate. However, the difference is negligible. The VSL command in section 1 converges to $v_1 = 30$ mi/h and the VSL command in section 9 converges to $v_9 = 55$ mi/h, which are not exactly the same as the desired values due to the application of the constraints.

In Fig. 9, ρ_9 and ρ_{10} converge to the corresponding equilibrium point in less than 10 min while ρ_1 converges to ρ_1^{e} much slower (in about 20 min). The reason of this phenomenon is the different values of ρ_1^{e} and ρ_9^{e}. As discussed in [1], a low value of speed limit would suppress the capacity of the section. After the incident occurs, v_1 decreases to a low value and ρ_1 increases rapidly, since because of the outflow of section 1, q_2 is suppressed by v_1. Then the process of adjusting ρ_1 from the overshoot to ρ_1^{e} takes long time due to the low level of q_2.

On the other hand, from Fig. 10, we can see that with the constrained VSL, ρ_1 converges fast and no overshoot is observed. This is because v_1 is constrained by (14) - (16) thus fails to adjust ρ_1 back to ρ_1^{e} after overshooting, however, as stated before, the difference is negligible. Similarly, in Fig. 10b, the VSL command v_1 converges to 30 mi/h in less than 10 min and stays at that value. Since the VSL commands only take whole 5 mi/h values due to (14), small variation of v_1 in the continuous case are all rounded up. Therefore, in the constrained case, there are no variations of v_1 around 30 mi/h.

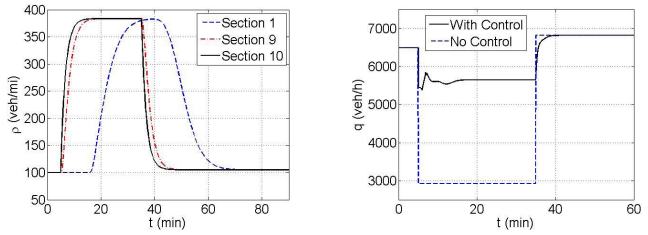

Fig. 11. (a) Vehicle Densities without Control; (b) Bottleneck Flow with and without Control.

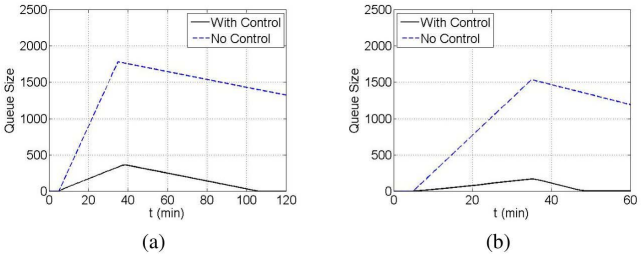

Fig. 12. Growth and Discharge of the Queue. (a) d = 6500 veh/h. (b) d = 6000 veh/h.

Fig. 11a demonstrates how vehicle densities evolve in scenario 1 without any control. The density increases dramatically in the discharging section to 370 veh/h and propagates upstream. Even after the incident is removed at $t = 35$ min, the shockwave continues propagating backwards and takes longer time to discharge. Fig. 11b shows the flow rate at the bottleneck with and without control. During the incident, the flow rate decreases to less than 3000 veh/h due to capacity drop in the case of no control, while the bottleneck flow converges to 5600 veh/h with the combined VSL and LC controller. Again, the flow rate under control is higher than the real capacity of the bottleneck due to the assumption of triangular fundamental diagram.

We use scenario 1 to examine the growth of the queue at the entrance to the controlled network. The numbers of vehicles in the queues are plotted in Fig. 12 with respect to the time t. When the demand $d = 6500$ veh/h, the maximum number of vehicles in the queue is 1700 in the case of no control, while the number is less than 500 in the control case, which demonstrates that the combined VSL and LC controller reduces the queue size significantly. The queues grow slower and discharge faster with lower demand, as less vehicles arrive at the tail of the queue.

C. Microscopic Simulation

In this section, we use a microscopic traffic model that is closer to the real environment in order to confirm the improvements predicted by theory and demonstrated by the macroscopic model. In addition, the microscopic model allows us to evaluate additional performance criteria such as number of stops and lane changes that affect safety as well as the environmental impact of VSL and LC controllers. We simulate the I-710 traffic flow network shown in Fig. 8 for the above mentioned 3 traffic scenarios. The simulated demand consists

TABLE I
EVALUATION RESULTS OF SCENARIO 1

Demand	6000 veh/h					6500 veh/h				
Control	No Control	LC Only	VSL Only	Control	Improvement	No Control	LC Only	VSL Only	Control	Improvement
T_t	18.85	17.12	18.95	16.85	-10.59%	20.72	17.67	21.21	16.83	-18.76%
$\bar{s}$	11.16	2.45	3.61	1.90	-83.00%	12.10	2.55	3.78	1.91	-84.21%
$\bar{c}$	4.00	4.75	4.74	3.78	-5.60%	4.67	5.54	5.88	4.31	-7.71%
NOx	1.56	1.49	1.61	1.49	-4.43%	1.64	1.58	1.60	1.53	-6.71%
CO2	558.56	543.22	577.59	536.01	-4.04%	589.46	556.47	605.59	537.21	-8.86%
Energy	178.65	173.67	184.76	171.40	-4.06%	186.78	177.93	193.73	170.31	-8.82%
PM25	0.049	0.048	0.047	0.050	0.66%	0.054	0.054	0.053	0.050	-7.73%

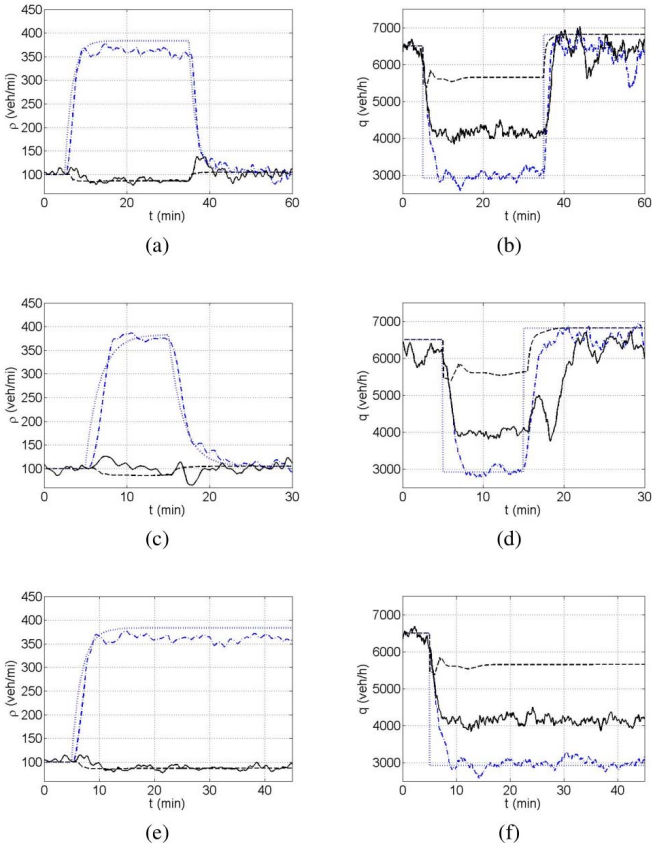

Fig. 13. Comparison of Macroscopic and Microscopic Models. -.-. Microscopic without Control. ... Macroscopic without Control. ___ Microscopic with Control. - - - Macroscopic with Control. (a) ρ_{10} in scenario 1. (b) q_b in scenario 1. (c) ρ_{10} in scenario 2. (d) q_b in scenario 2. (e) ρ_{10} in scenario 3. (f) q_b in scenario 3.

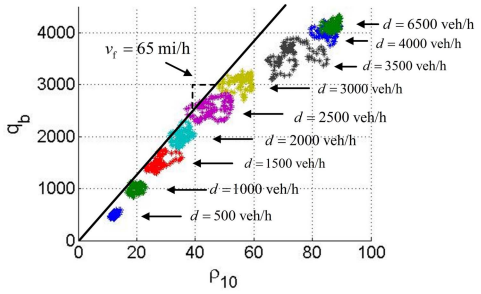

Fig. 14. Fundamental Diagram with Combined Controller.

of 85% light duty passenger vehicles and 15% trucks. This ratio represents the highest truck ratio at peak hours on I-710, therefore shows the worst traffic condition [35]. To show consistency of the results, we conducted 10 sets of Monte-Carlo simulations with different random seeds for each scenario. The curves in Fig. 13 are generated from a single simulation. The evaluation results in TABLE I - III are the average of 10 simulations.

1) Consistency Between Microscopic and Macroscopic Models: Fig. 13 shows the density and flow rate of the discharging section in both microscopic and macroscopic simulations. We can see that the density curve in macroscopic and microscopic simulations match each other. The microscopic flow rates in the no control cases are very similar and consistent with those in macroscopic simulations. However, when the combined VSL and LC controller is applied, the flow rates in microscopic simulations are lower than those in macroscopic simulations, which means that the flow speed in the discharging section in microscopic simulations is lower than what we get from the macroscopic model.

The deviation in speed is due to the following factors:

1) *Modeling error.* In the macroscopic model, we use a simplified triangular fundamental diagram to model the discharging section, which implies that the flow speed at the desired density is v_f. However, the actual speed would be lower than v_f. Especially when the LC controller is applied, drivers are usually conservative when merging to the open lanes.
2) *Speed limit following delay*. In the macroscopic model, we assume that the flow speed follows the speed limit exactly with no delay. However, in the microscopic model, the traffic flow needs time and space to accelerate to the desired speed limit. When vehicles change lanes, they do not adjust to new speeds instantaneously.
3) *Friction effect*. The friction effect reflects the empirically observed drivers' fear of moving fast in the open lanes when an incident or slowly moving vehicles exist in neighboring lanes [36]. In microscopic simulation, this phenomenon is captured and has an effect when compared with the macroscopic simulations.

Fig. 14 demonstrates the relationship between ρ_{10} and q_b at the equilibrium state under the combined VSL and LC controller in microscopic simulations. In Fig. 14, the negative slope part, i.e. the congested part of the fundamental diagram is not observed even when the demand d is higher than the

TABLE II
EVALUATION RESULTS OF SCENARIO 2

Demand	6000 veh/h					6500 veh/h				
Control	No Control	LC Only	VSL Only	Control	Improvement	No Control	LC Only	VSL Only	Control	Improvement
$\bar{T}_\mathrm{t}$	12.41	11.87	13.46	11.63	-6.25%	13.58	12.62	15.02	12.42	-8.54%
$\bar{s}$	5.16	0.75	2.16	0.65	-87.37%	5.72	1.58	2.33	0.91	-84.09%
$\bar{c}$	3.68	3.80	3.90	3.52	-4.31%	4.27	4.81	5.01	3.91	-8.33%
NOx	1.42	1.41	1.44	1.39	-2.48%	1.48	1.49	1.51	1.42	-4.05%
CO2	483.37	479.17	497.81	470.16	-2.73%	508.13	504.16	524.36	487.18	-4.12%
Energy	154.53	151.65	159.18	150.36	-2.70%	161.04	161.15	167.66	154.18	-4.26%
PM25	0.041	0.041	0.041	0.041	-0.77%	0.046	0.047	0.047	0.045	-2.17%

TABLE III
EVALUATION RESULTS OF SCENARIO 3

Demand	6000 veh/h					6500 veh/h				
Control	No Control	LC Only	VSL Only	Control	Improvement	No Control	LC Only	VSL Only	Control	Improvement
$\bar{T}_\mathrm{t}$	19.84	17.25	18.16	16.69	-15.89%	21.25	16.75	20.45	16.55	-22.13%
$\bar{s}$	15.46	2.13	4.00	1.74	-88.75%	16.12	2.54	3.72	1.83	-88.65%
$\bar{c}$	4.61	4.55	5.11	4.21	-8.60%	4.58	5.36	6.36	4.10	-10.48%
NOx	1.58	1.51	1.58	1.50	-4.95%	1.58	1.55	1.66	1.50	-4.95%
CO2	570.72	538.41	564.54	529.76	-7.18%	568.96	550.32	597.94	523.25	-8.04%
Energy	182.55	172.17	180.58	169.39	-7.21%	182.85	175.99	191.26	168.11	-8.06%
PM25	0.052	0.047	0.047	0.050	-3.74%	0.052	0.053	0.053	0.050	-3.74%

capacity, since the controller protects the bottleneck from getting congested. For different levels of demand, the data points concentrate in different clusters which shows that the controller homogenizes the traffic flow. Furthermore, when $d \leq 3000$ veh/h, the data points stay close to the line with the slope $v_\mathrm{f} = 65$ mi/h. When d keeps increasing, the data points move to the right side of the line due to the factors we explained above.

2) Performance Measurement and Criteria: We use the following measurements to evaluate the performance of the proposed controller. To be precise, in scenario 1 and 2, the measurements start at the time instant that the incident begins ($t = 5$ min) and terminate at the time instant 10 minutes after the incident ends ($t = 45$ min in scenario 1 and $t = 25$ min in scenario 2), so that the traffic states can achieve steady state. In scenario 3, where the incident is not removed, the measurements start at the time instant that the incident begins ($t = 5$ min) and terminate at $t = 45$ min. In each scenario, we collect the data of all vehicles that pass through the bottleneck during the above defined measuring periods and calculate the following values: (a)Average travel time $\bar{T}_\mathrm{t}$. (b)Average number of stops $\bar{s}$. (c)Average number of lane changes $\bar{c}$. (d)Average fuel consumption rate. (e)Average CO2 emission rate. (f)Average NOx emission rate. (g)Average PM25 emission rate. Control effects on traffic mobility are evaluated using the average travel time. Let N_v denote the number of vehicles pass through the bottleneck during the measuring period. Average travel time $\bar{T}_\mathrm{t}$ is defined as

$$\bar{T}_\mathrm{t} = \sum_{i=1}^{N_\mathrm{v}} (t_{i,\mathrm{out}} - t_{i,\mathrm{in}})/N_\mathrm{v}$$

where $t_{i,\mathrm{in}}$ and $t_{i,\mathrm{out}}$ denote the time instant vehicle i enters and exits the network respectively. Note that our simulation network has enough space upstream of the controlled segment, therefore the time waiting in the queue is also counted.

Control effects on traffic safety are evaluated by the average number of stops and average number of lane changes. Less stops and lane changes indicate smoother traffic flow and lower probability of crash [20]. $\bar{s}$ and $\bar{c}$ are defined as

$$\bar{s} = \sum_{i=1}^{N_\mathrm{v}} s_i/N_\mathrm{v}, \quad \bar{c} = \sum_{i=1}^{N_\mathrm{v}} c_i/N_\mathrm{v}$$

where s_i, c_i are number of stops and lane changes performed by vehicle i respectively. For environmental impact, we measure the average fuel consumption rate and the average emission rates of CO2, NOx, and PM25. These rates are uniformly defined as:

$$R = \sum_{i=1}^{N_\mathrm{v}} E_i / \sum_{i=1}^{N_\mathrm{v}} d_i$$

where E_i denotes the fuel consumed or a certain type of emission generated by vehicle i in the highway network, d_i represents the distance traveled by vehicle i in the network, and R denotes the fuel consumption rate or the tailpipe emission rate of CO2, NOx, or PM25. The fuel consumption rate and emission rates are calculated using the MOVES model of the Environment Protection Agency (EPA) based on the speed and acceleration profile of each vehicle [37].

3) Evaluation Results: TABLE I, II and III demonstrate the results of microscopic evaluation of all 3 scenarios under different traffic demands. From the results, we can see that the combined VSL & LC controller is able to provide significant improvements in traffic mobility, safety and environment. For traffic mobility, the proposed controller reduces the average travel time of each vehicle by 6.25% - 22.13%.

For traffic safety, the combined VSL and LC controller dramatically decreases the average number of stops by 83% - 88.75% in different scenarios, therefore drastically reduces the instances of the stop-and-go traffic, smooths the traffic flow

and damps the shockwaves. Average number of lane changes is also decreased by 5.6% - 10.48%. The combined VSL and LC controller homogenizes the density and speed in each section. Drivers tend to not change lane if densities and speeds are similar in all lanes, therefore the VSL control reduces the number of lane changes in the network under consideration. This is highly important for traffic safety in highway segments with high truck ratio. Trucks not only take long time and large space to change lane, their large size also blocks the eye sight of drivers, which makes lane changes of trucks much more dangerous than other vehicles.

The proposed controller reduces the fuel consumption rate and tailpipe emission rate from two perspectives. First, it reduces the travel time of vehicles, therefore decreases the emission levels of vehicles waiting in the queue. Second, it smooths the traffic flow and suppresses the acceleration and deceleration, therefore decreases the emission in these transient states. In the simulation, fuel consumption rate is decreased by 4.26% - 8.82%. The improvement in CO_2 emission rate is approximately proportional to the improvement of fuel consumption rate, since CO_2 is the main product of fuel burnt. The proposed controller reduces NO_x emission rate by about 3.54% - 6.71%. The emission rate of PM25 is also decreased by 3.74% - 7.73%. Therefore, the combined VSL and LC controller is able to bring environmental benefits.

The question how much of these improvements is due to VSL and LC controller alone is also answered using these simulation studies. From TABLE I - TABLE III, we can see that when the LC controller is applied alone, all evaluation criteria improve except for the average number of lane changes. The improvements on T_t and $\bar{s}$ are significant, while other criteria are only improved slightly. As discussed in Section II-C, the LC controller is able to recommend upstream vehicles to make lane changes before stopping at the queue and avoid the capacity drop therefore reduce the average travel time and average number of stops. Improvements on environmental criteria are results of improvements of traffic mobility. However, for the average number of lane changes, the LC controller only makes the lane changes take place in advance, instead of avoiding them, thus fails to reduce $\bar{c}$. Furthermore, when the VSL controller is applied alone, only the average number of stops is reduced. Other criteria are not improved and in some cases are even deteriorated by the VSL controller. This is because the VSL controller (10) is designed based on the assumption that the capacity drop has already been removed by the LC controller. When the LC controller is absent, VSL is not able to improve the bottleneck flow and reduce the vehicle density. But when the VSL controller is applied together with the LC controller, all criteria are further improved since the VSL stabilizes the vehicle densities at the desired equilibrium point and homogenizes the traffic flow. When the traffic flow is homogenized in each section and lane, the drivers do not tend to change lanes frequently, hence the average numbers of lane changes are also reduced.

Comparing the three scenarios, the improvement on each measurement criteria in scenario 2 appears to be less significant than the other 2 scenarios. The reason is that the incident duration in scenario 2 is very short.

V. Conclusion

In this paper we propose, analyze and evaluate a combined variable speed limit and lane change control strategy for highway traffic. In the proposed method, LC control provides lane change recommendations based on the bottleneck formation and traffic demand in order to remove capacity drop at the bottleneck. A nonlinear VSL controller is designed using a feedback linearization technique and shown to guarantee exponential convergence to the desired equilibrium states of density and speed that guarantee maximum flow at the bottleneck. Certain constraints on the VSL demands are imposed by taking into account driver response to VSL commands. Both macroscopic and microscopic simulations of the traffic along I-710 where the volume of trucks is relatively high are used to demonstrate improvements in travel time and the environment under different scenarios.

References

[1] R. C. Carlson, I. Papamichail, and M. Papageorgiou, "Local feedback-based mainstream traffic flow control on motorways using variable speed limits," *IEEE Trans. Intell. Transp. Syst.*, vol. 12, no. 4, pp. 1261–1276, Dec. 2011.

[2] A. Muralidharan and R. Horowitz, "Computationally efficient model predictive control of freeway networks," *Transp. Res. Part C, Emerg. Technol.*, vol. 58, pp. 532–553, Sep. 2015.

[3] H.-Y. Jin and W.-L. Jin, "Control of a lane-drop bottleneck through variable speed limits," *Transp. Res. Part C, Emerg. Technol.*, vol. 58, pp. 568–584, Sep. 2015.

[4] J. Zhang, H. Chang, and P. A. Ioannou, "A simple roadway control system for freeway traffic," presented at the Proc. Amer. Control Conf., Minneapolis, MN, USA, Jun. 2006.

[5] H. Chang, Y. Wang, J. Zhang, and P. A. Ioannou, "An integrated roadway controller and its evaluation by microscopic simulator vissim," in *Proc. Eur. Control Conf. (ECC)*, Jul. 2007, pp. 2436–2441.

[6] C. Roncoli, I. Papamichail, and M. Papageorgiou, "Hierarchical model predictive control for multi-lane motorways in presence of vehicle automation and communication systems," *Transp. Res. Part C, Emerg. Technol.*, vol. 62, pp. 117–132, Jan. 2016.

[7] Y. Zhang and P. A. Ioannou, "Combined variable speed limit and lane change control for truck-dominant highway segment," in *Proc. IEEE 18th Int. Conf. Intell. Transp. Syst. (ITSC)*, Sep. 2015, pp. 1163–1168.

[8] R. C. Carlson, I. Papamichail, and M. Papageorgiou, "Comparison of local feedback controllers for the mainstream traffic flow on freeways using variable speed limits," *J. Intell. Transp. Syst.*, vol. 17, no. 4, pp. 268–281, 2013.

[9] G.-R. Iordanidou, C. Roncoli, I. Papamichail, and M. Papageorgiou, "Feedback-based mainstream traffic flow control for multiple bottlenecks on motorways," *IEEE Trans. Intell. Transp. Syst.*, vol. 16, no. 2, pp. 610–621, Apr. 2015.

[10] A. Hegyi, S. P. Hoogendoorn, M. Schreuder, H. Stoelhorst, and F. Viti, "Specialist: A dynamic speed limit control algorithm based on shock wave theory," in *Proc. 11th Int. IEEE Conf. Intell. Transp. Syst.*, Oct. 2008, pp. 827–832.

[11] M. Abdel-Aty, J. Dilmore, and A. Dhindsa, "Evaluation of variable speed limits for real-time freeway safety improvement," *Accident Anal. Prevention*, vol. 38, no. 2, pp. 335–345, Mar. 2006.

[12] Z. Li, P. Liu, W. Wang, and C. Xu, "Development of a control strategy of variable speed limits to reduce rear-end collision risks near freeway recurrent bottlenecks," *IEEE Trans. Intell. Transp. Syst.*, vol. 15, no. 2, pp. 866–877, Apr. 2014.

[13] S. K. Zegeye, B. De Schutter, H. Hellendoorn, and E. Breunesse, "Reduction of travel times and traffic emissions using model predictive control," in *Proc. Amer. Control Conf. (ACC)*, Jun. 2009, pp. 5392–5397.

[14] B. Khondaker and L. Kattan, "Variable speed limit: A microscopic analysis in a connected vehicle environment," *Transp. Res. Part C, Emerg. Technol.*, vol. 58, pp. 146–159, Sep. 2015.

[15] L. D. Baskar, B. D. Schutter, and H. Hellendoorn, "Model-based predictive traffic control for intelligent vehicles: Dynamic speed limits and dynamic lane allocation," in *Proc. Intell. Vehicles Symp.*, Jun. 2008, pp. 174–179.

[16] Y. Zhang and P. A. Ioannou, "Environmental impact of combined variable speed limit and lane change control: A comparison of MOVES and CMEM model," *IFAC-PapersOnLine*, vol. 49, no. 3, pp. 323–328, 2016.
[17] T. Santos, J. Maria, D. Rosas, and F. Soriguera, "Evaluation of speed limit management on c-32 highway access to barcelona," in *Proc. 90th Annu. Meeting Transp. Res. Board*, 2011, p. 2397.
[18] K. Gao, "Multi-objective traffic management for livability," MS thesis, TU Delft, Delft, The Netherlands, 2012.
[19] L. Kejun, Y. Meiping, Z. Jianlong, and Y. Xiaoguang, "Model predictive control for variable speed limit in freeway work zone," in *Proc. 27th Chin. Control Conf.*, Jul. 2008, pp. 488–493.
[20] P. Ioannou, Y. Wang, A. Abadi, and V. Butakov, "Dynamic variable speed limit control: Design, analysis and benefits," METRANS Transportation Center, Los Angeles, CA, USA, Tech. Rep. METRANS 11-14, 2012.
[21] J. R. D. Frejo, A. Núñez, B. De Schutter, and E. F. Camacho, "Hybrid model predictive control for freeway traffic using discrete speed limit signals," *Transp. Res. Part C, Emerg. Technol.*, vol. 46, pp. 309–325, Sep. 2014.
[22] E. R. Müller, R. C. Carlson, W. Kraus, and M. Papageorgiou, "Microsimulation analysis of practical aspects of traffic control with variable speed limits," *IEEE Trans. Intell. Transp. Syst.*, vol. 16, no. 1, pp. 512–523, Feb. 2015.
[23] M. Papageorgiou, E. Kosmatopoulos, and I. Papamichail, "Effects of variable speed limits on motorway traffic flow," *Transp. Res. Rec., J. Transp. Res. Board*, no. 2047, pp. 37–48, 2008.
[24] Y. Wang and P. Ioannou, "New model for variable speed limits," *Transp. Res. Rec., J. Transp. Res. Board*, no. 2249, pp. 38–43, 2011.
[25] E. Van den Hoogen and S. Smulders, "Control by variable speed signs: Results of the dutch experiment," in *Proc. 7th Int. Conf. Road Traffic Monitor. Control*, Apr. 1994, pp. 145–149.
[26] J. H. Banks, "The two-capacity phenomenon: Some theoretical issues," *Transp. Res. Rec.*, no. 1320, pp. 234–241, 1991.
[27] F. L. Hall and K. Agyemang-Duah, "Freeway capacity drop and the definition of capacity," *Transp. Res. Rec.*, no. 1320, pp. 91–98, 1991.
[28] W.-L. Jin, "A multi-commodity Lighthill–Whitham–Richards model of lane-changing traffic flow," *Transp. Res. Part B, Methodol.*, vol. 57, pp. 361–377, Nov. 2013.
[29] J. A. Laval and C. F. Daganzo, "Lane-changing in traffic streams," *Transp. Res. Part B, Methodol.*, vol. 40, no. 3, pp. 251–264, Mar. 2006.
[30] M. Kontorinaki, A. Spiliopoulou, C. Roncoli, and M. Papageorgiou, "Capacity drop in first-order traffic flow models: Overview and real-data validation," in *Proc. 95th Annu. Meeting Transp. Res. Board*, 2016, p. 3541.
[31] C. F. Daganzo, "The cell transmission model: A dynamic representation of highway traffic consistent with the hydrodynamic theory," *Transp. Res. Part B, Methodol.*, vol. 28, no. 4, pp. 269–287, Aug. 1994.
[32] *VISSIM 5.30-04 User Manual*, PTV-Vision, Karlsruhe, Germany, Feb. 2011.
[33] H. K. Khalil and J. Grizzle, *Nonlinear Systems*. Englewood Cliffs, NJ, USA: Prentice-Hall, 1996.
[34] X.-Y. Lu, P. Varaiya, R. Horowitz, D. Su, and S. E. Shladover, "A new approach for combined freeway variable speed limits and coordinated ramp metering," in *Proc. 13th Int. IEEE Conf. Intell. Transp. Syst. (ITSC)*, Sep. 2010, pp. 491–498.
[35] C. D. of Transportation. (2015) *Caltrans Performance Measurement System (PeMS)*. [Online]. Available: http://pems.dot.ca.gov/
[36] M. Wright, G. Gomes, R. Horowitz, and A. A. Kurzhanskiy. (Sep. 2015). "A new model for multi-commodity macroscopic modeling of complex traffic networks." [Online]. Available: https://arxiv.org/abs/1509.04995
[37] *Motor Vehicle Emission Simulator (Moves) User Guide*, US Environ. Protection Agency, Washington, DC, USA, 2014.

Yihang Zhang received the B.S. and M.S. degrees from Northwestern Polytechnical University, Xi'an, China, in 2010 and 2013, respectively. He is currently working toward the Ph.D. degree with the Center of Advanced Transportation Technology, University of Southern California, Los Angeles, CA, USA. His research topics include the control of nonlinear systems, intelligent transportation systems, and highway traffic flow control and optimizations.

Petros A. Ioannou (S'80–M'83–SM'89–F'94) received the B.Sc. degree (Hons.) from University College London, London, U.K., in 1978, and the M.S. and Ph.D. degrees from University of Illinois at Urbana–Champaign, Champaign, IL, USA, in 1980 and 1982, respectively. In 1982, he joined the Department of Electrical Engineering-Systems, University of Southern California, Los Angeles, CA, USA, where he is currently the A.V. Bal Balakrishnan Chair Professor. He is also the Director of the Center of Advanced Transportation Technologies, University of Southern California. He also holds courtesy appointments with the Department of Aerospace and Mechanical Engineering and the Department of Industrial and Systems Engineering. He is the Associate Director of Research with the METRANS Transportation Center, University of Southern California.

Dr. Ioannou is a fellow of the IEEE, the IFAC and the IET. He received the Outstanding Transactions Paper Award from the IEEE Control System Society in 1984, the 1985 Presidential Young Investigator Award for his research in adaptive control, the IEEE ITSS Outstanding ITS Application Award in 2009, the 2009 IET Heaviside Medal for Achievement in Control from the Institution of Engineering and Technology, the IEEE ITSS Outstanding ITS Research Award in 2012, the 2016 IEEE Transportation Technologies Award in 2015.